4-3-2006

The *Arabidopsis* homolog of trithorax, ATX1, binds phosphatidylinositol 5-phosphate, and the two regulate a common set of target genes

Raul Alvarez-Venegas
University of Nebraska-Lincoln

Monther Sadder
University of Nebraska-Lincoln

Andrej Hlavacka
University of Bonn, Kirschallee 1, D-53115 Bonn, Germany

Frantisek Baluska
University of Bonn, Kirschallee 1, D-53115 Bonn, Germany

Yuannan Xia
Genomics Core Research Facility

See next page for additional authors

The *Arabidopsis* homolog of trithorax, ATX1, binds phosphatidylinositol 5-phosphate, and the two regulate a common set of target genes

Raul Alvarez-Venegas*, Monther Sadder*†, Andrej Hlavacka‡, František Baluška‡, Yuannan Xia§, Guoqing Lu*¶, Alexey Firsov*, Gautam Sarath‖, Hideaki Moriyama, Joseph G. Dubrovsky††, and Zoya Avramova*‡‡**

*School of Biological Sciences, University of Nebraska, Lincoln, NE 68588-0118; ‡Department of Plant Cell Biology, Institute of Botany, University of Bonn, Kirschallee 1, D-53115 Bonn, Germany; §Genomics Core Research Facility and ¶Bioinformatics Core Research Facility, Center for Biotechnology, University of Nebraska, Lincoln, NE 68588-0665; ‖United States Department of Agriculture, Agricultural Research Service Unit, East Campus, University of Nebraska, Lincoln, NE 68583-0939; **Department of Chemistry, University of Nebraska, Lincoln, NE 68588-0304; and ††Instituto de Biotecnología, Universidad Nacional Autónoma de México, Apartado Postal 510-3, Cuernavaca Morelos, CP 62250, Mexico

Communicated by Jeffrey L. Bennetzen, University of Georgia, Athens, GA, February 7, 2006 (received for review October 12, 2005)

The *Arabidopsis* homolog of trithorax, ATX1, regulates numerous functions in *Arabidopsis* beyond the homeotic genes. Here, we identified genome-wide targets of ATX1 and showed that ATX1 is a receptor for a lipid messenger, phosphatidylinositol 5-phosphate, PI5P. PI5P negatively affects ATX1 activity, suggesting a regulatory pathway connecting lipid-signaling with nuclear functions. We propose a model to illustrate how plants may respond to stimuli (external or internal) that elevate cellular PI5P levels by altering expression of ATX1-controlled genes.

epigenetic regulation | lipid signaling

Proteins of the trithorax family activate the early homeotic genes that regulate animal development and embryonic pattern formation (1, 2). A major difference in the developmental process in plants is that organ formation is not restricted to the embryonic state, differentiation and organogenesis occurring throughout the lifespan of the organism. In plants, as in animals, homeosis is a consequence of a mutation of a homeotic gene. Usually, homeotic genes encode transcription factors. Unlike the animal counterparts, however, many of the plant homeotic genes belong to the MADS-box family (3). Despite the difference in structure, plant homeotic genes, like animal counterparts, are controlled by factors belonging to the trithorax family (4). Mutation of the *Arabidopsis* homolog of trithorax, ATX1, causes numerous developmental defects in the formation, placement, and identity of flower organs: Petals (second-whorl organs) were seen to develop stems, a third-whorl feature; stamens (third-whorl organs) developed ovules, a fourth-whorl characteristic (4).

The signature feature of all trithorax proteins is the presence of the highly conserved SET [SuVar (3–9)-E(z)-trithorax] domain. The discovery that the SET domain peptides carry histone methyltransferase activity (5) provided critical evidence that chromatin-modifying activities function as epigenetic regulators. Certain lysines at the histone tails can be either acetylated or methylated, creating recognition sites for cellular repressive or activating complexes (6). SET domains of the trithorax family can methylate lysine 4 of histone H3, a modification associated with transcriptional activation (7). The SET domain of ATX1 has histone H3–K4 methyltransferase activity and can activate expression of *Arabidopsis* genes (4, 8). Thus, biochemical and genetic evidence define *ATX1* as a functional homolog of the animal *trithorax* genes.

Regulation of homeotic genes is only one possible role for trithorax (9, 10). In *Arabidopsis*, *atx1* mutants displayed stem-, root-, and leaf-growth defects, indicating that the plant homolog of trithorax has pleiotropic roles (4). By whole genome expression profiling, we determined that ≈1,700 genes changed robust expression as a result of ATX1 loss of function. The altered expression of these genes provides a probable molecular basis underlying the pleiotropic functions of ATX1.

The most important result of the study reported here is the finding that ATX1 can specifically bind the lipid messenger phosphatidylinositol 5-phosphate, PI5P. Phosphatidylinositol phosphates, PtdInsP, are important components of the cell lipid pool that function as intracellular and intercellular messengers in processes mediating plant growth, development, cytoskeletal rearrangements, and signal transduction (11). The inositol phospholipids can penetrate both hydrophilic and hydrophobic environments and can travel between, and within, cells. Existence of diverse phosphorylated isomers creates selective means for communication and for coordinating cell growth (12). The monophosphorylated isoform, PI5P, is a distinct minor component of the cellular inositol phospholipid pool that increased its levels in response to hyperosmotic stress (13). It may serve as a precursor for phosphatidylinositol bisphosphates, $PI3,5P_2$ and $PI4,5P_2$, whose syntheses also increase rapidly when yeast, animal, and plant cells respond to hyperosmotic stress (13–15).

Here, we show that the ATX1 interacts with PI5P and that the ATX1-PHD finger is involved in the binding. The plant homeodomain (PHD) peptide is a highly conserved motif, found in many nuclear and chromatin proteins (16). The PHD fingers belong to several families and may have different functions. For example, the PHD domain of the putative tumor suppressor (ING2) bound PI5P, and to a lesser extent PI3P, whereas the PHD of the repressor Mi2 did not bind any of the tested lipids (17). The PHD fingers of the polycomb-like protein were involved in protein-protein interactions (18), whereas the PHD finger of the ACF1 factor bound to histones (19). Trithorax family proteins carry one or more PHD fingers (20); the PHD of ATX1 belongs in a group defined as extended PHD (21) with unknown function.

Exogenous PI5P and ATX1 colocalized inside cells and elevated PI5P shifted ATX1 subcellular location. Identification of a distinct set of genes coregulated by ATX1 and PI5P provided biological relevance for their interaction. PI5P negatively affected ATX1 activity, suggesting that the epigenetic factor was regulated by the ligand. Based on our results, we propose a model of how plants may respond to stimuli that elevate cellular PI5P levels by altering expression in ATX1-controlled genes.

Results

Whole Genome Expression Analyses of *atx1* Mutants: The Large Number of Affected Genes Support Pleiotropic Roles of ATX1. We analyzed genome-wide expression of *atx1* mutant plants at bolting

Conflict of interest statement: No conflicts declared.

Abbreviations: ATX1, *Arabidopsis* homolog of trithorax; ING, putative tumor suppressor; PI4P, phosphatidylinositol 4-phosphate; PI5P, phosphatidylinositol 5-phosphate; PLO, protein lipid-blot overlay; PMA, 4-α-phorbol 12-myristate 13-acetate; PtdIns, phosphatidylinositol; SET, SuVar (3–9)-E(z)-trithorax.

†Present address: Faculty of Agriculture, University of Jordan, Amman 11942, Jordan.

‡‡To whom correspondence should be addressed. E-mail: zavramova2@unl.edu.

when root, leaf, and flower genes were expressed. The hybridization data for the *atx1* samples reported here were obtained as part of a larger experiment involving two additional experimental samples. Results from the robust expression analysis of genes affected by treatment with two lipid signaling molecules (PI5P and phosphatidylinositol 4-phosphate, PI4P) are not included in this study (R.A.V., Y.X., G.L., and Z.A., unpublished work), but relevant issues are discussed. The total numbers of genes detected in eight independent hybridizations (four samples, each tested in duplicate) consistently detected 60% (≈14,800) of all *Arabidopsis* genes expressed at this developmental stage. In an experiment performed 10 months later, the numbers of detected genes were 61.8% and 62.9% in control samples. The consistency in gene-detection numbers over a long time span confirmed the validity of our data. Quality and reproducibility of the GeneChip hybridizations are shown in Fig. 6, which is published as supporting information on the PNAS web site. Approximately 12% of the active genes at this stage of *Arabidopsis* development were affected by the ATX1 loss of function. Approximately 860 genes showed higher expressions, whereas 780 genes showed lower expressions, when compared with wild-type controls (Tables 1 and 2, which are published as supporting information on the PNAS web site).

***Arabidopsis* Genes Influenced by ATX1 Loss of Function: Overall Analysis.** Loss of ATX1 function affected a broad spectrum of genes involved in cellular and organismal processes (Fig. 7, which is published as supporting information on the PNAS web site). The largest proportion of impacted genes was involved in metabolic and physiological processes, followed by genes involved in stimuli response, cell communications, and apoptosis. Distribution of *atx1* genes with robustly altered expression, according to the subcellular localization of encoded products (based on the assigned Gene Ontology Cellular Component ID numbers), is summarized in Table 2, and discussion of *atx1*-down-affected and *atx1*-up-affected genes is available as *Supporting Text*, which is published as supporting information on the PNAS web site. Members of the same gene families were found with both positively and negatively modulated expression levels, underscoring the selectivity of the ATX1 targets, the specificity of its effects, and the fact that members of the same gene family could be antagonistically affected by the same regulator.

ATX1 Is Not a Constitutively Nuclear Protein. Transiently expressed *Arabidopsis* SET domain GFP fusion proteins localized in the nuclei of onion cells, in accordance with their presumed chromatin functions (22). Surprisingly, in cells of transgenic lines stably expressing the ATX1-GFP, the fusion protein was observed in the cytoplasm, along the plasma membrane, inside the cytoplasm, and, occasionally, into the nuclei (Fig. 1). This observation suggested that ATX1 was not a constitutively nuclear component. Next, we examined the presence of ATX1 in isolated nuclei. Immunostaining with anti-ATX1-specific antibodies revealed that only some nuclei stained positively for ATX1 (Fig. 8*A*, which is published as supporting information on the PNAS web site). Nuclei devoid of ATX1 stained positively for histone H4, indicating that lack of ATX1 was not an artifact of a general protein loss (Fig. 8 *B* and *C*). When in the nucleus, ATX1 was associated with chromatin overlapping with both DNA and with histone H4 (Fig. 8*D*).

The subcellular localization of ATX1 was nonuniform, suggesting that it might be a tissue or cell-specific event (Fig. 1 *A–C*). In the external tiers of the columella and in the root cap sloughing cells (the final differentiation state of these cells), ATX1 was seen in the cytoplasm and around the nuclei, but rarely inside the nuclei (Fig. 1 *D–F*). Strong signals were documented in perinuclearly aggregated ATX1 in root cap sloughing cells and in the corical cells of the transition zone (Fig. 1 *F* and *H*). In the elongation zone, ATX1 was seen along the plasma membrane (Fig. 1*I*, arrowheads). In the transition zone,

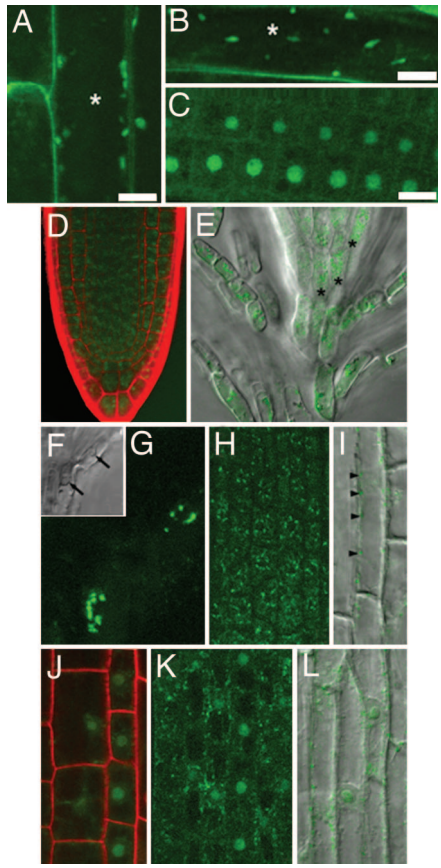

Fig. 1. Distribution of ATX1-GFP in *Arabidopsis* root cells and tissues. (*A–C*) Root cells from transgenic plants expressing ATX1-GFP. *, position of the nuclei in cells where ATX1 was not nuclear. (*D*) In all cell types of recently emerged lateral root, ATX1-GFP is in the cytoplasm. Cell walls are counterstained with propidium iodide. (*E*) ATX1-GFP localization in the root cap of primary root. In peripheral columella cells (*), ATX1 is dispersed throughout the cytoplasm, whereas, in the sloughing cells of the root cap, ATX1 is perinuclear (*F* and *G*). The nuclei are indicated by arrows. The image in *G* is *Z*-projection of eight optical sections, showing aggregates of ATX1 localized around the nuclei depicted in *F*. (*H*) *Z*-projection of five optical sections showing cytoplasmic and perinuclear localization of ATX1 in epidermal cells in the transition zone. (*I*) In epidermal cells of the elongation zone, ATX1 is detected along the plasma membrane (arrowheads); merged image of differential interference contrast microscopy (DIC) and *Z*-projection of four optical sections. (*J*) Nuclear localization of ATX1 in the epidermis within the transition zone. (*K*) Nuclear localization of ATX1 in the cortex (transition zone); *Z*-projection of nine optical sections. (*L*) Nuclear and membrane localization of ATX1 in the epidermis in the elongation zone; merged image of DIC and of a single optical section. *E–H*, *K*, and *L* were taken from the same root ($n = 26$).

ATX1 showed cytoplasmic (Fig. 1*B*), perinuclear, and nuclear localization (Fig. 1 *H* and *J*). Nuclearly localized ATX1 was found in the transition zone and in some rapidly elongating cells of the epidermis and cortex (Fig. 1 *J–L*). In the same roots, nuclearly localized ATX1 could be found in adjacent files, or in a file, surrounded by neighbors depleted of nuclear ATX1 (Fig. 1*K*).

The surprisingly variable localization of ATX1 within the cells suggested that the protein was dynamically relocating. We hypothesized that ATX1 localization was a development- and/or environment-related phenomenon and that presence of ATX1 in different cellular subcompartments reflected changes in response to internal and/or external signals.

ATX1 Specifically Binds the Phospholipid PI5P. The idea that ATX1 could bind lipid ligands was suggested by the strong similarity of the

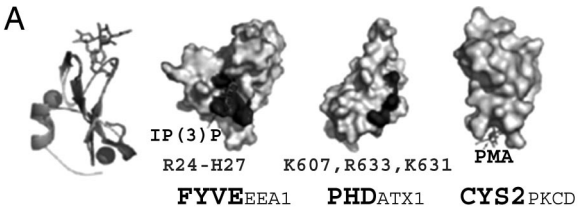

B

```
                                        Zn2 _____       Zn1
ATX    PHD  590  grhqnqptgyrpvrvDWKDLDKCNVCHMDEEYENNLFLQCDKCR---MMV
ING2   PHD  193  kakqereASPVEFAIDPNEPTYCL-CNQVSYGEMIG---CDNEQCPIEWF
EEA1   FYVE         1 RKWAEDNEVQNCMACGKGFSVTVRRHH-CRQC---GGVF
VSP27  FYVE       163 dsktpaDWIDSDACMICSKKFSLLNRKHH-CRSC--GMNV
CYS2   PKCD       231 HRFKVYNYMSPTFCDHCGSLLWGLVKQGLKCEDC---GMNV
Ruler           1-------10-------20--------30--------40--------50
                 Zn2                Zn1
ATX    PHD  637  HAKCYGELEPCDGAL-----WLCNLCRPGAPDMPPQcclcpv 673
ING2   PHD  239  HFSCVSLTYKPKGK------WYCPKCRGDNEKtndktkkerr 274
EEA1   FYVE  36  CAECSAKNALTP--SSKKPVRVCDACFNDLQG 67
VPS27  FYVE 100  CQECSSNSIPLPDLGIYEPVRVCDSCFEDYEFIVTD 235
CYS2   PKCD 269  HHKCREKVANLC 272
Ruler            51------60--------70--------80--------90--
```

Fig. 2. Structural models of PHD_{ATX1}, $C1_{PKC}$, and $FYVE_{EEA1}$. (*A*) Superposition of PHD_{ATX} peptide model (residues 599–648) on the structure of the Cys-2-domain (25). The ligand, DAG/PMA (black sticks), binds in a cleft formed between two loops. In the surface models of $FYVE_{EEA1}$ (PDB 1HY), PHD_{ATX} (residues 606–667), and $CYS2_{PKCD}$ (PDB 1PTR), the basic patches are dark. The PI3P binding to $FYVE_{EEA1}$ and PMA binding to $CYS2_{PKCD}$ are shown in black sticks. (*B*) Alignment of zinc-finger sequences belonging to different PHD families. Zinc coordination residues are shown in black-shaded white fonts. Light-shaded residues are involved in the positive patches at the PI3P-binding sites in VPS27, EEA1 (26), ING2 (17).

ATX1–PHD finger with C1-domain peptides known as lipid ligand receptors (23). ATX1 amino acids 586–662 carry the sequence: $HX_{19}CX_2CX_{13}CX_2CX_4HX_2CX_6C$, similar to the C1-domain consensus sequence, $HX_{12}CX_2CX_{13}CX_2CX_4HX_2CX_7C$ (24). C1 peptides (i.e., the $C1_{PKC}$ domain of protein kinase C) bind diacylglycerol (DAG)/phorbol esters. However, the extended PHD of ATX1 is similar also to the Fab1p, YOTB, Vac 1p, EEA1 (FYVE)-peptide motifs, a specific receptor for PI3P (25), and the PI5P-binding PHD_{ING2} (17) (Fig. 2*B*).

Simulated models for PHD_{ATX1} built on available data for $C1_{PKC}$ (26) and for $FYVE_{EEA1}$ (27) revealed conserved features (Fig. 2*A*). The superimposed structures of $C1_{PKC}$ (red) and PHD_{ATX1} (blue) showed that the peptides might share similar coordination of two Zn^{2+} atoms connected by two strands of β sheets. DAG/4-α-phorbol 12-myristate 13-acetate (PMA) binds the C1 domain in a cleft (26) conserved also in PHD_{ATX1}. However, a tryptophan residue (W606) inside the substrate-binding pocket in PHD_{ATX1} makes it shallower. This modification might be responsible for the inability of ATX1 to bind PMA *in vitro* (see In Vitro *Binding Assays*). A basic motif (the RKHH motif) conserved in the structure of all FYVE-containing proteins (27), and the (3K motif) in ING2 (17) forms a pocket required for the ligand binding. In the PHD_{ATX1} model, the amino acids K_{607}, K_{631}, and R_{633}, form a basic motif of a similar size as that of FYVE and ING2 fingers (≈12 Å; surface model) capable of accommodating a PtdInsP ligand of ≈11 Å, the length of PI5P.

***In Vitro* Binding Assays.** To establish whether ATX1 has a true lipid-binding activity, we tested 16 lipids and PtdInsPs prespotted onto membranes by the protein lipid-blot overlay (PLO) assay (17, 28). After incubating the membranes with recombinant GST-ATX1, followed by GST antibodies to identify bound protein molecules, only one spot yielded a signal (Fig. 3*A*). The spot corresponded to PI5P, indicating a very high specificity of the interaction. Experiments with serially diluted PtdInsPs further confirmed the specificity of the binding (Fig. 3*B*). As controls, we tested two peptides with previously established ligand-binding specificities. We expressed the PX domain, a specific PI3P receptor, and the PHD_{ING2} finger, binding PI5P and PI3P (17, 26) as GST fusion proteins and tested ligand binding in parallel with GST-ATX1. In agreement with reported specificities, the PX peptide bound only PI3P, whereas the PHD_{ING2} finger showed a broader specificity, binding PI5P, PI3P, and PI4P (Fig. 3 *D* and *E*). GST-ATX1 bound exclusively PI5P.

To define the region involved in the binding, we generated and tested deleted versions of ATX1. Removal of the entire N-terminal half of ATX1 did not affect the lipid binding; the SET domain alone (amino acids 909-1020, without preSET and postSET regions) did not bind PI5P, whereas the extended PHD (ePHD)-SET-postSET

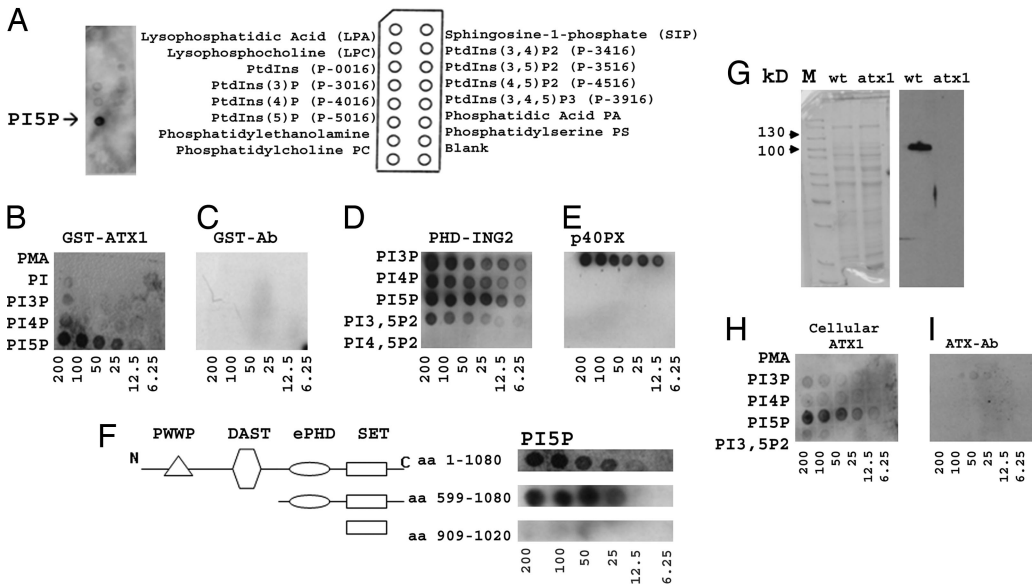

Fig. 3. *In vitro* ligand binding by the protein-lipid overlay (PLO) assays. (*A*) Binding of recombinant GST-ATX1 to prespotted lipids. A key is shown to the right. (*B*) Affinity purified GST-ATX1 fusion protein reacted with membranes containing serially diluted ligands, as indicated: PMA, 4-α-phorbol-12-myristate-13-acetate; PI, phosphatidylinositol (PtdIns); PI3P, PtdIns(3)P; PI4P, PtdIns(4)P; PI5P, PtdIns(5)P; PI3,5P_2, PtdIns(3,5)P_2; P4,5P_2, PtdIns(4,5)P_2. Substrate concentrations in picomoles are shown. Bound proteins were revealed by GST-specific antibodies. (*C*) Duplicate control membrane reacted with the GST antibody. (*D* and *E*) Binding of recombinant GST-PHD_{ING2} and GST-p40PX to membranes containing tested ligands. (*F*) PI5P-binding activity of GST-ATX1 and various deletion GST-fusion peptides. (*G*) Coomassie-stained SDS gels of total cellular proteins extracted from wild-type plants and from *atx1* mutants. Western blot of the same extracts with the ATX1-specific antibody. Absence of the band in *atx1* mutants confirms the specificity of the antibody. (*H* and *I*) Cellular ATX1 binds PI5P. Replicate membrane reacted with the ATX antibodies as a control for the specificity of the signal.

peptide bound PI5P as strongly as the whole protein (Fig. 3*F*). The results implicate ePHD in the binding of PI5P to ATX1.

Although the similarities in sequence and in tertiary structures between PHD_{ATX1} and $C1_{PKC}$ suggested that ATX1 might be able to bind phorbol esters as well, PLO assays did not detect PMA binding with either recombinant or cellular ATX1 (Fig. 3 *B* and *H*). In separate experiments using an alternative protocol (24), we tested a labeled phorbol ester analogue ([^{3}H]phorbol 12,13-dibutyrate). No phorbol ester-binding activity of ATX1 *in vitro* was detected by this approach (data not shown).

Cellular ATX1 also Binds Preferentially PI5P. To determine whether cellular ATX1 would display affinities similar to the recombinantly expressed proteins, we reacted total cell extracts from 3-week-old plants with membranes carrying prespotted PtdIns and PMA. Ligand-bound ATX1 was identified with antiATX1-specific antibodies (Fig. 3*G*). The result illustrated that ATX1 within its "native" context also bound exclusively to PI5P (Fig. 3*H*).

Genes Coregulated by ATX1 and PI5P: Biological Relevance of the ATX1-PI5P Interaction. To determine whether binding of ATX1 to PI5P might be relevant for *Arabidopsis* function, we analyzed gene expression affected by the two molecules. An overlapping set of common targets would imply that PI5P and ATX1 work together in the plant. To estimate the specificity of the targets, we analyzed gene overlaps with genomes of plants treated with PI4P, a lipid that did not bind ATX1 in PLO assays.

Cluster analyses of whole genome expression profiles of PI5P-treated and of *atx1* mutant plants identified ≈240 common genes: 138 down-regulated and 99 up-regulated (Figs. 9 and 10 and Table 3, which are all published as supporting information on the PNAS web site). Statistical analysis showed a significant coregulation between *atx1* and PI5P. The Pearson correlation coefficient is 0.59 ($P < 0.0001$, $n = 100$) for up-regulated genes, whereas the coefficient is 0.47 ($P < 0.0001$, $n = 133$) for down-regulated genes. Only five genes were affected in opposite direction: two genes were PI5P up-regulated but *atx1* down-regulated, and three genes were PI5P down-regulated but *atx1* up-regulated. Because PI5P affected similarly (up or down) the expression of the shared genes as ATX1 loss of function, we concluded that PI5P negatively controls wild-type ATX1. Distribution of overlapping genes according to assigned Gene Ontology Cellular Component and Gene Ontology numbers are summarized in Table 2 and Fig. 9.

The specificity of a PI5P–ATX1 pathway was estimated by cluster analyses of *atx1*-affected and PI4P-affected genes. Shared genes in the PI5P/*atx1* and PI4P/*atx1* fractions would illustrate points of convergence of the two pathways. Venn diagrams indicated that PI5P and PI4P participate in distinct mechanisms and regulate largely nonoverlapping sets; only 17 genes (1 up-regulated and 16 down-regulated) were found in the overlap (Fig. 10).

ATX1 Shifts Localizations in Response to Increased PI5P Concentrations. The ability of a ligand to mobilize a receptor protein is a criterion for their interactions *in vivo* (23). Consequently, we followed the shift of nuclear ATX1-GFP caused by exogenously added PI5P (Fig. 4). Time-lapse observations over a period of 95 min registered that some nuclei decreased signals, whereas other nuclei lost it almost completely (Fig. 4*A Bottom*). The results suggested that elevated PI5P could mobilize ATX1. When treated with PI4P, a lipid that did not bind ATX1 *in vitro*, the signal remained nuclear.

Western blot analysis confirmed these observations (Fig. 4*C*). In mock-treated root cells, ATX1 was detected in both the cytoplasmic and the nuclear fractions. After exposure to PI5P, the nuclear ATX1-specific band visibly diminished, whereas exposure to PI4P did not cause a similar effect, supporting the idea of a dynamic relocation of nuclear ATX1 after exposure to PI5P. Apparently, nuclear and cytoplasmic ATX1 fractions represent the same protein that shifts locations rather than two different entities. Cytoplasmic ATX1 bands were reproducibly stronger, suggesting that endogenous PI5P might favor cytoplasmic localization of ATX1.

A red-tagged derivative of PI5P was used to test whether PI5P colocalized with ATX1-GFP inside cells. An overlap was seen at some, but not all, intracellular locations (Fig. 4*B*), reinforcing the idea that the two interact in cells *in vivo*. Nonoverlapping signals might suggest that ATX1 has been complexed with endogenous PI5P before addition of exogenous PI5P.

A Model for Plants' Responses to External/Internal Stimuli. Based on our results, we propose a model of a plausible mechanism for the plants' response to environmental and developmental stimuli (Fig. 5). Plants respond to elicitors that increase the concentration of PI5P (13) by altering expression of relevant genes. Expression of ATX1-regulated genes is, ultimately, controlled by availability and concentrations of PI5P. In cases of genes stimulated in *atx1* mutants, the function of wild-type ATX1 would be to silence these genes by keeping active a repressor until developmental and/or environmental conditions initiate response. Depending on its concentration in the cell, PI5P could instruct derepression of growth-promoting genes by deactivating ATX1. The model illustrates a pathway that translates environmental and developmental stimuli along a messenger (PI5P)-receptor (ATX1) pathway into altered expression of the common target gene set.

Discussion

ATX1 Functions as a Positive and as a Negative Regulator of *Arabidopsis* Gene Expression. Approximately 1,640 genes altered expression in *atx1* mutants, indicating that ATX1 regulates func-

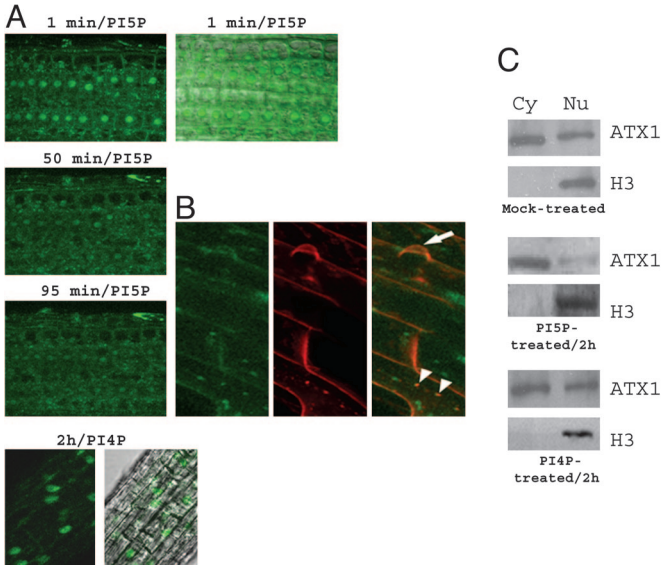

Fig. 4. ATX1 in cells of *Arabidopsis* roots after treatment with PtdIns. (*A*) PI5P-induced changes in localization of ATX1-GFP. Time lapse experiments of roots treated with 1.5 μM of PI5P. Images taken 1 min, 50 min, and 95 min after drug application show *Z*-projections of 10, 9, and 10 optical sections, respectively. (*A Top*) The image on the right represents a merge of the (1 min) left image with the differential interference contrast microscopy (DIC) image. (*Middle*) After 95 min, most nuclei in the lower file of cells have almost completely lost nuclear signal. In contrast, exposure to PI4P for up to 2 h did not trigger loss of nuclear signal. (*A Bottom*) Right image is a merge of DIC with the image on the left. (*B*) Red particles inside root epidermis cells show presence of BODIPY^R TMR-PI5P inside cells. Localization of ATX1-GFP protein is seen in green. Images shown in green and red channels are taken 30 min after treating roots in media supplied with 1.5 μM of red-tagged PI5P. (*B Right*) A merged image. Colocalization at the membrane (orange) may be seen along cell walls, particularly at the bulge of the emerging root hair (arrow). Inside the cytoplasm, PI5P is colocolized with ATX1 protein particles (some spots are shown by arrowheads). (*C*) Western blots of cytoplasm (Cy) and nuclear (Nu) proteins with ATX1 specific antibodies.

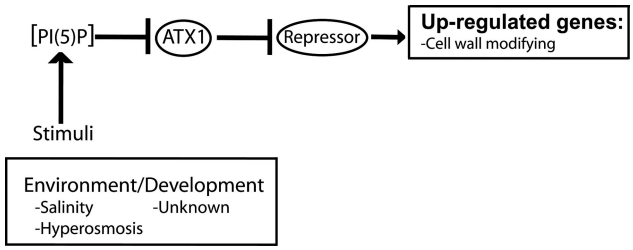

Fig. 5. A model of a PI5P-ATX1 signaling pathway controlling *Arabidopsis* genes. Developmental and environmental factors influence the cellular concentration of PI5P. Higher levels of PI5P deactivate ATX1, which, in turn, represses transcription factors, a repressor in the case of some wall-modifying genes. Arrows, activation; T-shaped bars, repression events.

tions beyond the homeotic genes. About equal numbers of genes decreased or increased expression as a result of ATX1 loss of function defining wild-type ATX1 as an activating and as a repressive factor in *Arabidopsis*. This result was unexpected because trithorax factors and histone H3-lysine 4 methylations, in general, are associated with gene activation (2, 6, 7). It is likely that some genes are secondary targets of ATX1 reflecting altered expression of pertinent transcription factors. Indeed, ≈60 genes encoding transcription factors were misexpressed (42 activated and 18 silenced) in the *atx1* mutants. Earlier, we showed that tissue-specific transcription factors have a dominant control of expression over histone modification patterns (8). Direct silencing by ATX1 is also a possibility that deserves to be explored. For instance, epigenetic factors previously associated only with activation (histone acetyltransferases) were found to repress transcription directly (29).

ATX1 is not responsible for genome-wide methylation of histone H3-K4 (8), and microarray data provided further support that ATX1 targeted specific genes. Even within the same family, ATX1 affects selected members. The results imply that same-family genes are under specific control of multiple mechanisms. Different complexes might be recruited in response to specific stimuli to target selectively individual family members, ensuring specific responses to developmental and environmental cues.

ATX1 Is a Receptor for the Lipid Messenger PI5P. Microarray hybridization, biochemical, and microscopic data provide evidence that ATX1 acts as a receptor for the PI5P ligand in *Arabidopsis*.

ATX1 and PI5P Interact Specifically and Control a Set of Shared Genes. The common set of genes in ATX1 and in PI5P-treated plants provided evidence for *in vivo* interactions between ATX1 and PI5P. PI5P, alone, affected ≈360 genes, and ≈70% of its targets were coregulated with ATX1. For the remaining genes, PI5P participates in pathways bypassing ATX1. On the other hand, ATX1 controls genes by a mechanism not involving PI5P.

Distribution of the common set of genes (Fig. 9) outlined a pattern of affected functions similar to that displayed by PI5P alone: ≈55% and 56% of PI5P- and PI5P/*atx1*-affected genes, respectively, were involved in metabolism, whereas, in the *atx1*, the respective fraction constituted 33%. Cellular and organismal physiological processes were more affected in *atx1* mutants (≈40%) than by PI5P alone (≈20%) of all impacted genes. In the overlap, ≈20% of the genes were involved in these functions. It is interesting to note also the differences in the proportion of genes involved in response to stimuli (10% in PI5P; 9.3% in the overlap; 5.6% in *atx1*) and in cell communication (2.8% in *atx1*; 9.3% in PI5P; 8.7% in the overlap). Thereby, overall distribution level analyses revealed that effects triggered by PI5P were largely mediated by ATX1 (see *Supporting Text* for more discussion).

We found also that ≈70 genes were coregulated by ATX1 and PI4P, despite the fact that ATX1 did not bind detectably PI4P. This fact suggests that ATX1 interacts indirectly with PI4P. It is plausible, then, that ATX1 functions in a complex with receptors for other ligands (30). Modularly organized receptor complexes would provide highly specific responses.

The ATX1-PI5P coregulated gene set is distinct from the set coregulated by ATX1-PI4P (Fig. 10), suggesting that mechanisms involving either PI5P or PI4P target different genes. However, the two pathways may converge, in agreement with the idea that individual genes are under multiple controls.

The fact that *atx1* and PI5P controlled expression of 240 genes in the same direction (only five genes changed expression in opposite directions) indicates that, in the wild type, PI5P inactivates ATX1.

PI5P Is a Second Messenger in *Arabidopsis*. Increased salinity raised the levels of cellular PI5P in plants, triggering pathways involving inositol phospholipid bisphosphates synthesized from PI5P (13). However, it was unknown whether PI5P could act as a ligand on its own or whether its cellular function was solely to serve as a precursor for biphosphate messages. The fact that ATX1 binds PI5P, but not its derivatives ($PI4,5P_2$ and $PI3,5P_2$), argues that PI5P, itself, serves as a ligand. This conclusion does not preclude existence of other PI5P-involving pathways or a role for PI5P as a precursor for other signaling molecules. Among 360 PI5P-responding genes, only 240 overlapped with *atx1*-affected genes, suggesting that there are other PI5P receptors in *Arabidopsis.* On the other hand, ATX1 affects many genes beyond the overlap, indicating that a complex with PI5P is not the only route for ATX1.

Recombinantly expressed and cellular ATX1 preferentially bound PI5P (Fig. 3), but deletion of the PHD-SET regions aborted the binding. These facts, together with the postulated structure of the PHD finger, implicated the PHD domain in the interaction. There are other members of the trithorax family in *Arabidopsis* (20, 22), and it would be interesting to determine whether they can bind any PtdInsP.

ATX1 and PI5P Colocalize in Cells and PI5P Can Trigger an ATX1 Shift. As an epigenetic factor and chromatin modifier, ATX1 functions in the nuclei. However, its variable localization in different cellular subcompartments, even within cells of the same tissue, indicated that ATX1 did not reside permanently in the nuclei. Finding of ATX1 at the plasma membrane, around the nucleus, and inside the nucleus, suggests that the protein might shuttle between these compartments. Relocation could be triggered by internal or external signals. Shift of ATX1 to the cytoplasm after treatment with PI5P (confirmed also by Western blot assays) suggested that nuclear localization of ATX1 would depend on factors affecting the concentration of PI5P. The latter might be under cell cycle and/or developmental control. In murine cells, an increase in nuclear PI5P mass has been observed only in the G_1 phase of the cell cycle (31), suggesting that changes in the levels of PI5P might have major implications for the activity of ATX1 and the expression of the common target genes. The PI5P/*atx1* overlapping genes indicated that PI5P and ATX1 act antagonistically. At a cellular level, PI5P might sequester ATX1 inside the cytoplasm, preventing it from acting on the chromatin. The overlap of exogenously added PI5P and ATX1-GFP inside cells further support this idea. A precedent is class II histone deacetylases regulated by compartmentalization (32). At a structural level, binding of PI5P to ATX1 may induce a conformational change affecting ATX1 activity. The two mechanisms are not mutually exclusive.

Lipid Signaling and the Nuclear Proteins. Lipid signaling is involved in broader functions than a role at the plasma membrane. ATX1 does not bind the abundant plant PI4P, suggesting that ATX1 is not involved in stable complexes at the plasma membrane.

Lipid kinases have been found at the nuclear membrane and

the nuclear matrix, PI4,5P_2 has been found in heterochromatin, and inositol tetrakis-, pentakis-, and hexakisphoshate can bind chromatin modifying complexes (33–35), whereas PI5P regulates the tumor suppressor ING2 (17). Comparison of PI5P-caused effects suggests that PI5P may exhibit opposite affects on the activity of its different nuclear receptors. For example, the tumor suppressor ING2 detaches from chromatin and exits the nuclei at lowered levels of PI5P, indicating that PI5P positively affected ING2 activity (17). In contrast, nuclear ATX1 is excluded from the nuclei at elevated ligand concentrations, indicating that PI5P negatively effected ATX1 function.

Thereby, ATX1 links epigenetic regulation with lipid signaling by its ability to directly bind the ligand. However, this interaction might not be the only way in which the two processes are linked. For example, the ASH2 protein from the trithorax group in *Drosophila* interacts with a PI4,5P kinase to affect chromatin activity (30). Protein-protein interactions were reported also for the trithorax SET domain with members of the myotubularin family, MTM (36, 37). MTM proteins carry a dual-specificity phosphatase motif and a predicted SET domain-binding domain. The significance of a putative MTM-trithorax complex is not clear but suggests intriguing relationships and undiscovered pathways.

Materials and Methods

Plant Material and PtdIns Treatments. The *atx1* mutant line and a transgenic *atx1* line stably expressing the ATX1-GFP fusion protein, rescuing the *atx1* phenotype, were as described in ref. 4. D-*myo*-PI5P and D-*myo*-PI4P (Echelon Biosciences, Salt Lake City, UT) 1 mM stock solutions were made following the manufacture's instructions. Next, 10 μl of the stock dissolved in 10 ml of the germination media (final concentration of 1 μM), without the agar, were added to the growth media. Controls were treated with similarly diluted solute used for the lipid stock.

RNA Sample Preparation and Microarray Data Analyses. In two independent experiments, RNAs were isolated from *atx1* mutant, PI5P-treated, PI4P-treated, and mock-treated wild-type plants, grown and handled under the same conditions. Whole plants, grown for 20 h in the presence of exogenously added drug, were harvested and frozen in liquid nitrogen. In separate experiments, we have established that change of gene expression was stabilized over a period of 8- to 24-h exposure to the lipids (R.A.-V., Y.X., G.L., and Z.A., unpublished work). Samples were prepared following manufacturer's instructions (see *Supporting Text*).

Three experimental samples (PI5P-treated, PI4P-treated, and *atx1* mutant *Arabidopsis thaliana*) in hybridizations performed in duplicate were analyzed versus each of four independent control preparations from wild-type untreated plants (see *Supporting Text*). We wrote a computer program to identify genes significantly expressed in PI5P-treated and PI4P-treated samples when compared with wild type and to find overlapping genes that expressed significantly in PI5P-treated, PI4P-treated, and *atx1* mutant samples (see *Supporting Text*).

Recombinant fusion proteins GST-ATX1 and the various deleted versions, GST-SET and His-PHD-SET, were bacterially expressed and affinity purified (4). The plasmids expressing GST-p40PX and GST-PHD_{ING2} were expressed and purified following the same protocol.

Protein Lipid-Blot Overlay (PLO) Assays. PtdInsP were from Echelon BiosciencesPMA was from Sigma, and the labeled substrate ([H]phorbol 12,13-dibutyrate) was from ICN Biomedicals. Protein interaction assays were done as described (28).

Homology Modeling. Simulated models of the PHD_{ATX1} finger domain (residues 608–667) were built by using SWISS-MODEL, 3D-JIGSAW, and CCP4, based on reported structures for FYVE-zinc finger in VPS27 and DAG-zinc-finger of Cys-2 activator-binding domain in protein kinase Cδ (see *Supporting Text*).

Confocal Laser Scanning Microscopy. Living roots, unstained or stained for 5 min with 5 $\mu g \cdot ml^{-1}$ propidium iodide (Sigma), were analyzed under an upright Leica TCS4D (488 nm line of a Kr/Ar laser) and an inverted Zeiss LSM 510 Meta microscopes (see *Supporting Text* for details). C-05R16 BODIPY-PI5P-tagged product from Echelon Biosciences was used to illustrate internalization and colocalization of exogenous PI5P.

We thank Or Gozani (Harvard University) for providing the plasmids expressing the GST-PX and GST-PHD_{ING2} fusion proteins. We thank Mehtap Yielmaz for the pictures of the nuclei, S. Napsucialy-Mendivil and A. M. Saralegui for excellent technical help, and Y. Joe Zou from the University of Nebraska (Lincoln) microscope facility. The studies were supported in part by Universidad Nacional Autónoma de México, Project IN210202 (to J.G.D.) and National Science Foundation Grant MCB-0343934 (to Z.A.).

1. Mazo, A., Huang, D.-H., Mozer, B. & Dawid, I. (1990) *Proc. Natl. Acad. Sci. USA* **87,** 2112–2116.
2. Simon, J. A. & Tamkun, J. W. (2002) *Curr. Opin. Genet. Dev.* **12,** 210–218.
3. Schwartz-Sommer, Z., Huijser, P., Nacken, W., Saedler, H. & Sommer, H. (1990) *Science* **250,** 931–936.
4. Alvarez-Venegas, R., Pien, S., Sadder, M., Witmer, X., Grossniklaus, U. & Avramova, Z. (2003) *Curr. Biol.* **13,** 627–637.
5. Rea, S., Eisenhaber, F., O'Carroll, D., Strahl, B. D., Sun, Z.-W., Schmid, M., Opravil, S., Mechtler, K., Pontig, C. P., Allis, C. D. & Jenuwein, T. (2000) *Nature* **406,** 593–599.
6. Strahl, B. D.& Allis, C. D. (2000) *Nature* **403,** 41–45.
7. Milne, T. A., Briggs, S. D., Brock, H. W., Martin, M. E., Gibbs, D., Allis, C. D. & Hess, J. L. (2002). *Mol. Cell* **10,** 1107–1117.
8. Alvarez-Venegas, R. & Avramova, Z. (2005) *Nucleic Acids Res.* **33,** 1599–5207.
9. van Lohuizen, M. (1999) *Curr. Opin. Genet. Dev.* **9,** 355–361.
10. Sharples, N. & DePinho, R. (1999) *Curr. Opin. Genet. Dev.* **9,** 22–30.
11. Wang, X. (2004) *Curr. Opin. Plant Biol.* **7,** 329–336.
12. Stevenson, J. M., Perera, I. Y., Heilmann, I., Persson, S. & Boss, W. F. (2000) *Trends Plant Sci.* **5,** 252–258.
13. Meijer, H. J. G., Berrier, C. P., Iurisci, C., Divecha, N., Musgrave, A. & Munnik, T. (2001) *Biochem. J.* **360,** 491–498.
14. Dove, S. K., Cooke, F. T., Douglas, M. R., Sayers, L. G., Parker, P. J. & Michell, R. H. (1977) *Nature* **190,** 187–192.
15. Pical, C., Westergren, T., Dove, S. K., Larsson, C. & Sommarin, M. (1999) *J. Biol. Chem.* **274,** 38232–38240.
16. Aasland, R., Gibson, T. & Stewart, A. F. (1995) *Trends Biochem. Sci.* **20,** 56–59.
17. Gozani, O., Karuman, P., Jones, D. R., Ivanov, D., Cha, J., Lugovskoy, A. A., Baird, C. L., Zhu, H., Field, S. J., Lessnick, S. L., *et al.* (2003) *Cell* **114,** 99–111.
18. O'Connell, S., Wang, L., Robert, S., Jones, C. A., Saint, R. & Jones, R. S. (2001) *J. Biol. Chem.* **276,** 43065–43073.
19. Eberharter, A., Vetter, I., Ferreira, R. & Becker, P. B. (2004) *EMBO J.* **23,** 4029–4039.
20. Alvarez-Venegas, R. & Avramova, Z. (2002) *Gene* **285,** 25–37.
21. Linder, B., Newman, R., Jones, L. K, Debernardi, S. B., Young, D., Freemont, P., Verrijzer, C. P. & Saha, V. (2000) *J. Mol. Biol.* **299,** 369–378.
22. Baumbusch, L. O., Thorstensen, T., Krauss, V., Fischer, A., Naumann, K., Assalkhou, R., Schiltz, I., Reuter, G. & Aalen, R. B. (2001) *Nucleic Acids Res.* **29,** 4319–4333.
23. Ron, D.& Kazanietz, M. G. (1999) *FASEB J.* **13,** 1658–1676.
24. Ono, Y., Fuji, T., Igarashi, K., Kuno, T., Tanaka, C., Kikkawa,U. & Nishizuka, Y. (1989) *Proc. Natl. Acad. Sci. USA* **86,** 4868–4871.
25. Simonsen, A., Wirmser, A. E., Emr, S. D. & Stenmark, H. (2001) *Curr. Opin. Cell Biol.* **13,** 485–492.
26. Zhang, G., Kazanietz, M. G., Blumberg, P. M. & Hurley, J. H. (1995) *Cell* **81,** 917–924.
27. Kutateladze, T. & Overduin, M. (2001) *Science* **291**, 1793–1796.
28. Dowler, S., Kular, G. & Alessi, D. (2002) *Sci. STKE*, 10.1126/stke.2002.129.pl6.
29. Grienenberger, A., Miotto, B., Sagnier, T., Cavalli, G., Schramke, V., Geli, V., Mariol, M. C., Berenguer, H., Graba, Y. & Pradel, J. (2002) *Curr. Biol.* **12,** 762–766.
30. Cheng, M. K. & Shearn, A. (2004) *Genetics* **167,** 1213–1223.
31. Clarke, J. H., Letcher, A., D'Santos, C. S., Halsted, J. R., Irvine, R. F. & Divecha, N. (2001) *Biochem. J.* **357,** 905–910.
32. Yang, X.-J. & Seto, E. (2003) *Curr. Opin. Genet. Develop.* **13,** 143–153.
33. Jones, D. R. & Divecha, N. (2004) *Curr. Opin. Genet. Develop.* **14,** 196–202.
34. Shen, X., Xiao, H., Ranallo, R., Wu, W.-H. & Wu, C. (2003) *Science* **299,** 112–114.
35. Steger, D., Haswell, E. S., Miller, A. L., Wente, S. R. & O'Shea, E. K. (2003) *Science* **299,** 114–116.
36. Gui, X., de Vio, I., Slany, R., Miamoto, A., Firestein, R. & Cleary, M. L. (1998) *Nat. Genet.* **18,** 331–337.
37. Mochizuki, Y. & Majerus, P. (2003) *Proc. Natl. Acad. Sci. USA* **100,** 9768–9773.

Supporting Information

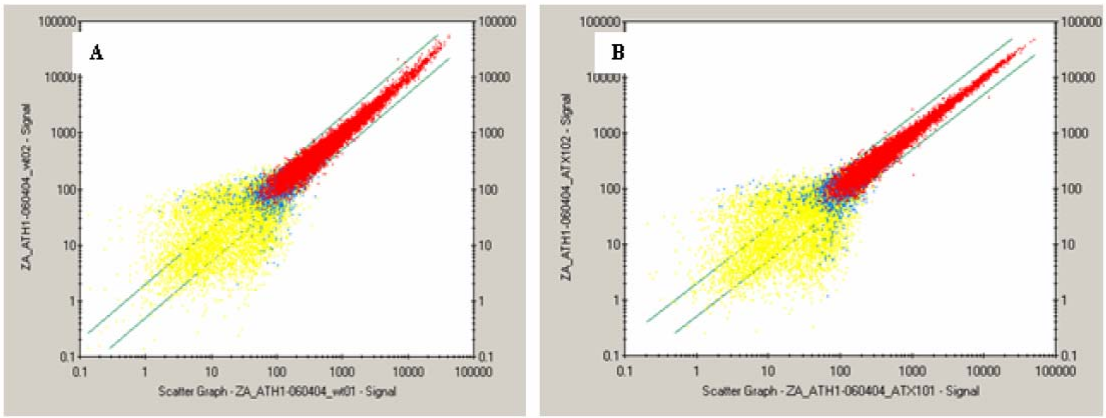

C

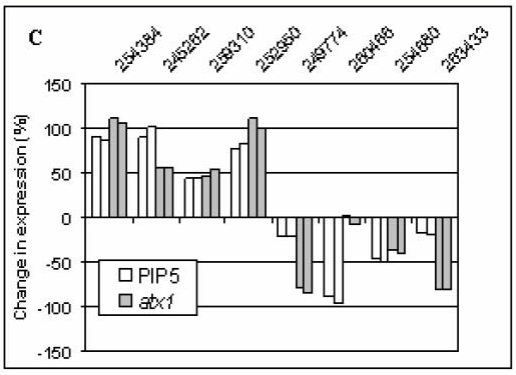

D

Probe set ID	Fold change atx1/WT	Fold change PI5P/mock	AGI
254384_at	10.00	4.03	At4g21870
245262_at	3.60	1.90	At4g16560
259310_at	1.57	1.55	At3g05160
252950_at	2.07	1.87	At4g38690
249774_at	-2.37	-1.78	At4g11280
260466_at	P-M	- 1.84	At1g10900
254680_at	-1.80	-1.84	At4g18130
263433_at	-1.60	-1.76	At2g22240

Fig. 6. Reproducibility and semiquantiative reverse-transcriptase PCR confirmation of the GeneChip hybridization data. Scatter plots comparing the raw signal intensities of two independent samples. (*A*) Wild type, untreated. (*B*) *atx1* mutant plants. Lines indicate two-fold change. Colors of the points represent different detections: yellow, A-A, A-M, M-A, and M-M; blue, A-P, M-P, P-A, and P-M; and red, P-P. A, absent; P, present; M, marginal (see *Supporting Text*). (*C*) RT-PCR analysis confirming data from the microarray hybridizations. Results from two independent amplification experiments are shown in tandem. The differences in band intensities, after subtracting the values from wild-type control samples, were plotted as percent change. Black columns, changed intensities in *atx1* samples; white columns, changes in expression of phosphatidylinositol 5-phosphate (PI5P) treated samples. The numbers on top are the Affymetrix identification numbers. (*D*) Data from the microarray hybridizations of the genes shown in the histogram.

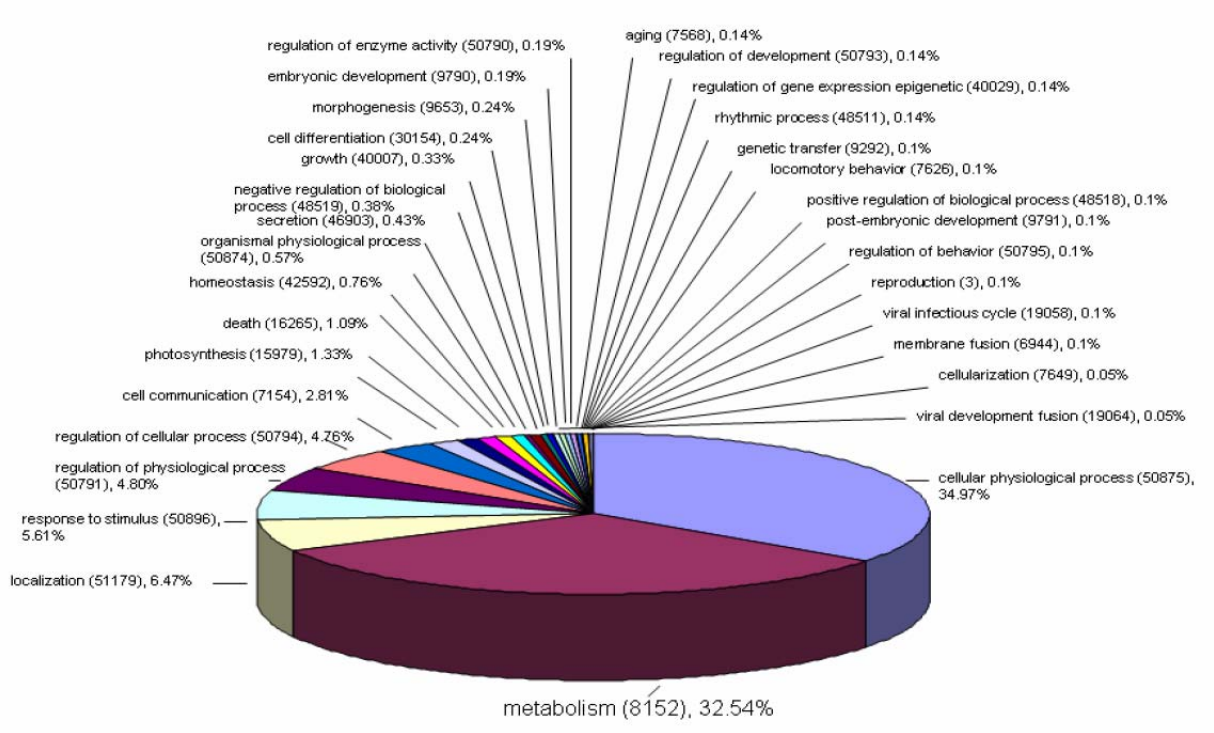

Fig. 7. Distribution of genes with altered expression resulting from ATX1 loss of function according to Gene Ontology (biological processes function).

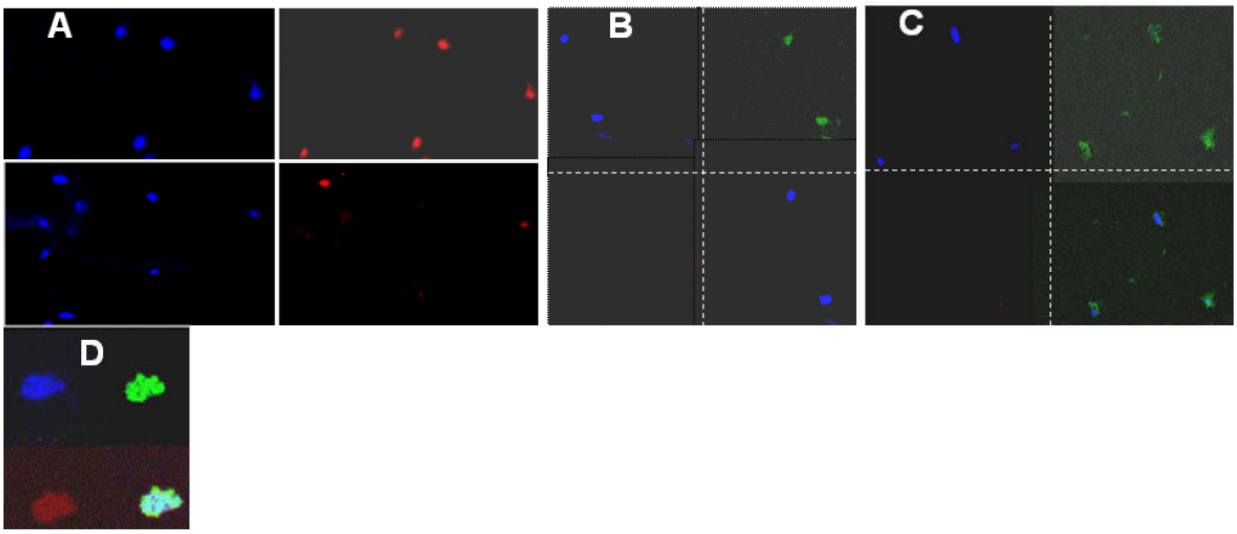

Fig. 8. Immunostaining of root cell nuclei for ATX1 showing that ATX1 is not a constitutively nuclear protein. Isolated root nuclei were stained with DAPI (blue), with anti-ATX1 antibodies (red), and with anti-histone H4 antibody (green). (*A*) In two different fields, nuclei positive for ATX1 (red) and void of ATX1 are shown. (*B* and *C*) ATX1-negative nuclei stain positively for histone H4 (green), indicating that lack of ATX1 signal was not an artifact of a general nuclear

protein loss. Broken white lines separate four optic fields carrying nuclei counterstained with DAPI (blue), Cy-5 (red), and Cy-2 (green). Right-hand bottom corner images show merged fields: in *B*, DAPI is merged with red; in *C*, DAPI is merged with green. (*D*) Enlarged image of a nucleus carrying ATX1 that overlaps with both DNA and histone H4.

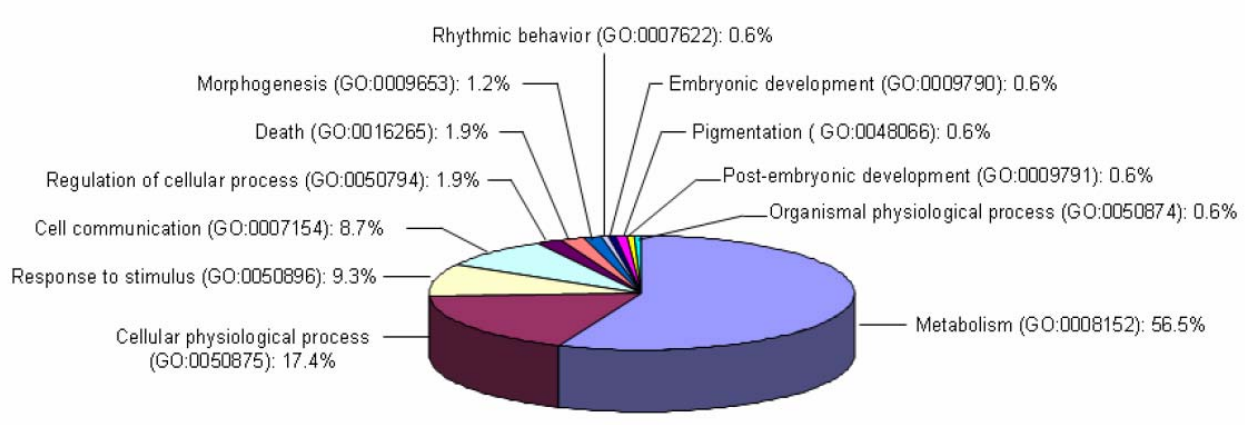

Fig. 9. Distribution of shared *atx1*/PI5P overlapping genes according to Gene Ontology (biological processes function).

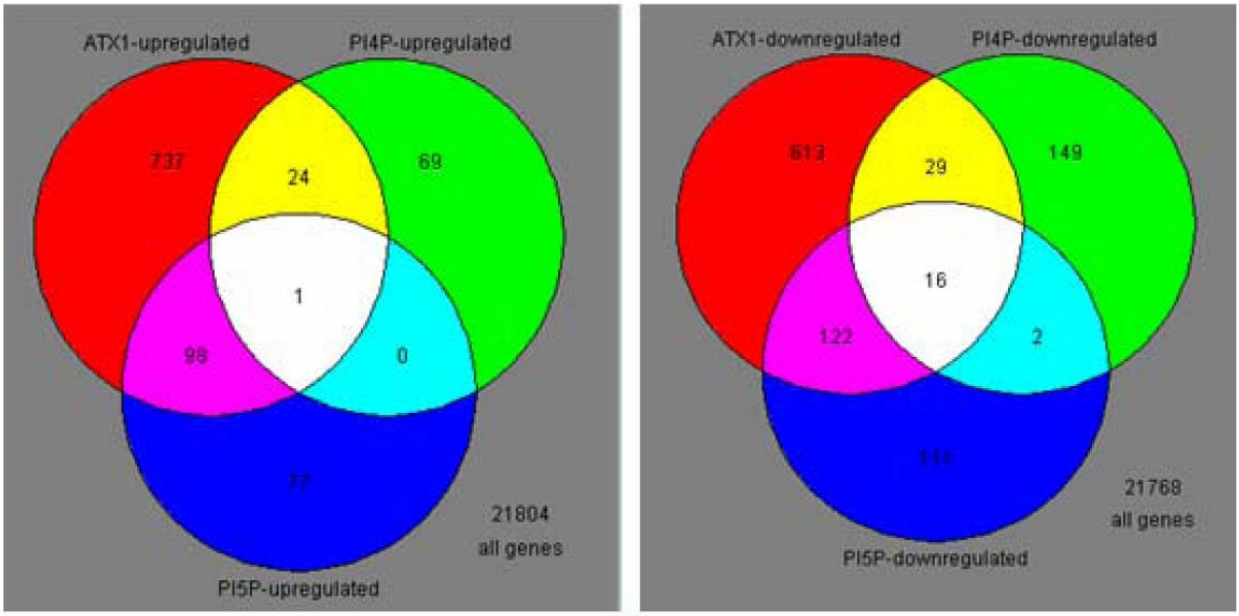

Fig. 10. Venn diagrams of overlapping genes with altered expression in the three samples. Significantly up-regulated and down-regulated genes in *atx1* mutants (marked as ATX1 on the diagrams) in phosphatidylinositol 5-phosphate (PI5P)- and phosphatidylinositol 4-phosphate (PI4P)-treated samples are represented *Left* and *Right*, respectively. Numbers in the overlaps show coregulated genes.

Supporting Text

Arabidopsis Homolog of Trithorax (*ATX1*)-Affected Genes

***atx1*-Downregulated Genes.** For ≈47% of all of the down-regulated genes, there was no predicted association with cellular substructures. Approximately 19% of the genes encoded chloroplast, 6% encoded mitochondrial, 4% encoded cytoplasm, and 6% encoded nuclear components. Eighteen percent encoded membrane- and wall-associated proteins. The majority of the latter activities represented ABC-type transporters, metal transporters, potassium-channel proteins, members of the cytochrome P450 family, and various enzymes involved in sugar and lipid metabolism. Only four genes (*At1g48100*, *At1g60590*, *At2g18660*, and *At5g65390*) from the group of the wall-architecture group were found in the repressed fraction, in contrast with the 18 genes up-regulated by the *atx1* mutation (see Table 1).

Genes involving protein kinases, phosphatases, and putative components of signal transduction pathways were also down-regulated. Repressed were two male sterility (MS5) family proteins, genes from the family of the late embryogenesis abundant (LEA) proteins, and numerous genes involved in responses to biotic and abiotic stresses (Table 1).

ATX1 loss of function negatively influenced expression of 49 genes encoding nuclear proteins; among them, 42 genes represented established and putative transcription factors. Highly represented were various families of Zinc finger (*ZF*-) transcription factors (17 genes), nine members of the *MYB*, seven of the *bHLH*, five of the *NAM*, and four of the *AP2*-box families. Three genes of the *WRKY* and three of the *MADS* box family had lower expression in the *atx1* samples. *HOMEOBOX*, *CONSTANS*, *HEAT SHOCK*, and *TCP* transcription families were represented in the silenced fraction by one or two genes each.

***atx1*-Induced Genes.** As a result of ATX1 loss of function, 861 genes augmented expression. For the products of 274 genes (32%), there was no predicted subcellular location. Approximately 6% of the genes encoded mitochondrial, 19% encoded chloroplast, 5% encoded cytoplasm, and 3% encoded nuclear components. Approximately 300 genes (34%) encoded endomembrane and cell wall-associated activities. Activated were genes involved in putative cellular transduction pathways, two-component signaling systems, protein kinases, and phosphatases, genes for defense response, disease resistance, heat shock, various stress responses, and apoptosis.

Overall, ATX1 equally activated and silenced genes encoding similar activities, except for transcription factor encoding genes, more genes (42) were silenced than activated (18) in *atx1* plants. In contrast, more genes encoding wall-architecture functions were activated than silenced in *atx1* mutants: 18 were up-regulated and 4 were down-regulated. Thereby, wild-type ATX1 mostly activated transcription factor genes but repressed many wall-architecture genes.

Different members of the same transcription factor family were found activated or repressed by the ATX1, underscoring selective targeting by ATX1.

Only some nuclei were ATX1 positive (Fig. 8*A*). Nuclear ATX1 was associated with chromatin overlapping with both DNA and with histone H4 (Fig. 8*D*). Nuclei void of ATX1 signal still stained positively for histone H4 (Fig. 8 *B* and *C*), indicating that lack of ATX1 signal was not an artifact of a general protein loss.

***atx1*/phosphatidylinositol 5-phosphate (PI5P)-Overlapping Genes.** ATX1 binds specifically PI5P *in vitro*; the two colocalize inside cells and regulate ≈240 common genes. It is logical to conclude that the two function together *in vivo*. This was confirmed by defining a common set of coregulated genes.

The subcellular localization of the products of the shared genes, according to the assigned Gene Ontology Cellular Component numbers, is summarized in Table 2. In the down-regulated fraction, we note the large overlap of genes encoding transcription factors. In addition, many genes involved in pathogen and various stress responses were also found among the shared target genes, as well as genes from the male sterility family, from the *LEA* gene family, and *RuBisCo* binding factors (Tables 1–3). The results suggest that PI5P and ATX1 act together to control reproductive, embryonic, light-, and drought-response systems.

In the up-regulated sets of genes, we note the large PI5P/*atx1* overlap of membrane-bound and cell wall-bound genes. Various endomembrane components (electron, ion, sugar, peptide, and oxygen) transporters, lipid transfer protein (LTP), redox activities, stress-related dehydrins, phosphate-induced proteins, and genes for carbohydrate metabolism, found in the overlap, agree with a postulated role of a PI5P-ATX1 complex in membrane and signaling functions. Up-regulated were also 19 of the 29 PI5P-activated wall-modifying genes, indicating that a significant number of wall-architecture activities are controlled by a mechanism employing both PI5P and ATX1.

When challenged by PI5P, wild-type plants responded mainly by silencing transcription factor genes. Among them, 21 genes were coregulated (activated) by ATX1. Thereby, elevated PI5P silenced expression of 21 transcription factor genes by negatively affecting ATX1 activity upon these shared genes. Clearly, some genes in the overlapping fractions represented secondary targets. Only three genes encoding transcription factors were found in the activated PI5P/*atx1* overlap.

Thereby, wild-type ATX1 activity PI5P silences three transcription factor genes and various endomembrane components (electron, ion, sugar, peptide, and oxygen) transporters, redox activities, stress-related dehydrins, phosphate-induced proteins, and genes for carbohydrate metabolism.

Whether PI5P participates in the hyperosmotic stress response as a precursor or as a ligand itself remains to be established. Many genes encoding stress-related dehydrins, heat shock-responsive, low temperature-responsive, pathogen-responsive, and desiccation-responsive factors, as well as apoptosis-related and LEA proteins, are present in the shared PI5P/*atx1* fraction (Table 3),

compatible with a conclusion that it is PI5P, rather than its derivatives, involved in the control of these genes.

Only five genes were affected in opposite direction: two genes up-regulated with PI5P but down-regulated in *atx1* (*At4g03400 and At5g66985*), and three down-regulated with PI5P but up-regulated in *atx1* (*At1g036550, At3g036500 and At3g18280*).

Specificity of the *atx1*/PI5P Pathway. In plant cells, phosphatidylinositol 4-phosphate (PI4P) was found widely distributed in various subcellular compartments, suggesting that the lipid might be involved in distinct physiological roles (1). Exposure to PI4P affected ≈280 genes: 88 genes up-regulated and 197 genes down-regulated, compared with mock-treated control samples (R.A.-V., Y.X., G.L., and Z.A., unpublished data). Sixty genes were found in the overlapping gene sets of *atx1* and PI4P-treated samples (35 genes down-regulated and 25 genes up-regulated). Because no binding interaction was detected between ATX1 and PI4P, the two, most likely, interact indirectly.

Materials and Methods

Semiquantitative Reverse-Transcriptase PCR Analysis. Total RNA was extracted from 0.3 g of tissue by using the BRL Trizol reagent and repurified with the Qiagen RNeasy Mini kit, following the manufacturer's instructions. Fifteen micrograms of total RNA was used to synthesize cDNA using One-cycle cDNA synthesis kit, according to the manufacturer's instructions (Affymetrix). All sample preparations followed prescribed protocols (Affymetrix GeneChip Expression Analysis Technical manual). Semiquantitative reverse-transcriptase PCR reactions were performed in a 20-μl volume containing 2.5 μg of total RNA and 200 units of the M-MLV Reverse Transcriptase from Invitrogen, following the manufacturer's conditions. The TaKaRa Ex-*Taq* polymerase was used during PCR, and the conditions were as follows: 95°C for 30 min, 60°C for 30 min, and 72°C for 1 h for 34 cycles.

Microarray Hybridization and Data Analyses. Hybridizations were done on an Affymetrix *Arabidopsis* genome ATH1 array, stained with streptavidin-phycoerythrin conjugate on an Affymetrix fluidics station 450, followed by scanning with the GeneChip scanner 3000 (Affymetrix). Affymetrix GeneChip Operating Software (GCOS) was used for washing, scanning, and basic data analysis.

The Affymetrix microarray contains more than 22,500 probe sets (≈24,000 genes). Each probe set consisted of 11 probe pairs with a perfect match (PM) sequence corresponding to a specific region of a gene. For each PM sequence, there was also a corresponding mismatch (MM) oligo that differs by one base. The AFFYMINER program was used for mining significant genes. The cutoff for average signal values between the experimental and control samples was 0.5, corresponding to ≈1.5-fold change in intensity levels.

The data were published in GCOS and used in Affimetrix Data Mining Tool (DMT) for the calculation of average signal value and fold change for each probe set. The data were exported to a Microsoft Excel file for identifying robust changes between the treatments and the controls. For each array, overall intensity normalization for the entire probe sets was preformed by using

the scaling approach, which adjusts the average intensity or signal value of every array to a common value to make the arrays comparable. The target signal intensity 500 was set up for scaling. Single array analysis generated a detection *P* value to determine the detection call, present (P) or absent (A). Additionally, a signal value, a relative measure of abundance to the transcript, was calculated. For comparison analysis, the array for wild type (WT) is designed as a baseline, and the arrays for PI5P treated or ATX1 mutant were designed as treatment. Instead of simply comparing signal values of each probe set, GCOS examines changes in the intensities of both PM and MM probes between the treatment and the baseline using a nonparametirc Wilcoxon rank test. However this method is available only for pair-wise array comparison.

We wrote a computer program to identify genes significantly expressed in PI5P-treated and PI4P-treated samples when compared with wild type and to find overlapping genes that expressed significantly in PI5P-treated, PI4P-treated, and in *atx1* mutant samples. The following criteria were used in our program: (*i*) detection call should be "present" in the two experiment replicates; (*ii*) change calls from the pair-wise comparisons should be all "I," i.e., increase, or "D," decrease; (*iii*) fold change of average signal values between the treatments and the controls should be no less than 1.5. Five genes showing extreme values of fold change have been excluded from statistical analysis when determining the Pearson correlation coefficient.

Protein Lipid-Blot Overlay (PLO) Assays. Phosphatidylinositol (PtdInsP) were from Echelon Biosciences (Salt Lake City, UT), 4-α-Phorbol 12-myristate 13-acetate (PMA) was from Sigma, and the labeled substrate ([^{3}H]phorbol 12,13-dibutyrate, [20-^{3}H]) was from ICN. Lyophilized lipids were reconstituted into a solution of methanol:chlorophorm:water (2:1:0.8) and stored at –80°C. Appropriately diluted samples were spotted onto Nitrocellulose Hybond-CExtra (Amersham Pharmacia Biosciences) membranes, dried at room temperature, and processed for protein interaction assays as described (9). Binding of cellular ATX1 to PtdIns was tested using the same protocol. The membranes loaded with lipid compounds were reacted with 0.5 ml cellular extract containing 50-100 ng of ATX1. ATX1 concentrations were estimated by comparing the intensity of the bands binding ATX antibodies in Western hybridizations with the intensity of bands from established amounts of recombinant ATX1 reacted with the same antibodies.

Image Analysis. Confocal laser scanning microscopy living roots, unstained or stained for 5 min with 5 μg ml^{-1} propidium iodide (Sigma), were analyzed under an upright Leica TCS4D (488 nm line of a Kr/Ar laser) and inverted Zeiss LSM 510 Meta microscopes. With a Zeiss microscope, a 543-nm line of a He/Ne laser and a 488-nm line of an Ar laser were used for propidium iodide and GFP excitation, respectively. GFP imaging was done with a BP 500-530 filter. Time-lapse recordings were done always under the same laser settings. To decrease bleaching, differential interference contrast microscopy (DIC) images were acquired with only 3% of laser force. Leica x63 and Zeiss x63 water immersion objectives were used. C-05R16 BODIPY-PI5P-tagged product from (Echelon Biosciences) was used to illustrate internalization and colocalization of exogenous PI5P. Images were captured with the Gel Doc 2000 gel documentation system and analyzed with the QUANTITY ONE software, both from Bio-Rad. To measure the amount of particular bands, a volume rectangle of the same size was created around each band of interest, and the intensity data (the sum of intensities of the pixels inside the volume boundary area) were compared with the data of other objects using the Volume Analysis Report via the global

background subtraction method. The results are reported as differences in intensity (INT) or as percentage, when compared to the wild-type samples.

AntiATX-Antibody Preparation and Immunostaining. Polyclonal antibodies against ATX1 were raised against a peptide (amino acids 355-388) divergent between ATX1 and ATX2. We have synthesized the 23 amino acid peptides and have generated rabbit antibodies (CoCalico Biologicals, Reamstown, PA). The final sera were concentrated and purified from contaminating RuBisCo antibodies by affinity chromatography. The ATX Ab (1:5000 dilution) reacted with only one protein band of ≈116 kDa in on Western blots. Total cell proteins were extracted by grinding frozen plant tissue (10 g) in liquid nitrogen and homogenization in 20 ml of plant protein extraction buffer (50 mM Tris·HCL, pH 8.0/100 mM $CaCl_2$/10% glycerol/30 mM 2-mercaptoethanol/5 mM PMSF/5 μg/ml aprotinin/5 μg/ml pepstatin). After incubation (10 min at room temperature), filtration (cheesecloth), and centrifugation (20 min at 14,476 × *g* in a Sorvall RC-5B, 4°C); the supernatant was precipitated with ammonium sulfate (80%, overnight, 4°C, followed by centrifugation for10 min at 14,476 × *g* in a Sorvall RC-5B, 4°C), the pellet was dissolved in 1-2 ml of water and dialysed overnight against buffer containing 50 mM Tris, pH 7.5 and 15 mM NaCl. Equal loading was monitored by measuring overall protein concentrations in each fraction using the Pierce Coomassie Plus reagent (Pierce).

Isolated nuclei were reacted with the primary ATX antibody (1-2 h at room temperature), washed with PBST (0.05% Tween 20/3% BSA), and incubated with Cy2, Cy3, or Cy5-conjugated secondary antibody (Jackson ImmunoResearch). Control samples were prepared with preimmune sera or with no primary antibody. Images were collected under a BioRad MRC1024ES confocal laser microscope using a dual excitation/emission (488 nm/640 nm and 522 nm/680 nm) imaging program. Antibodies against histone H4 (raised in donkeys) were used as immunostaining controls.

Nuclei isolation and immunostaining for ATX were performed following reported procedures (2). Roots of *Arabidopsis* seedlings expressing ATX1-GFP were observed under Zeiss LSM 510 Meta confocal microscope.

Homology Modeling. Simulated models of the ATX Zinc-finger domain (residues 608–667) were built based on reported structures for FYVE-Zinc finger in VPS27 (3) (PDB ID: 1VFY) and DAG-Zinc finger of Cys-2 activator-binding domain in protein kinase Cδ (4) by using SWISS-MODEL (5), 3D-JIGSAW (6), and CCP4 (7). Visual presentation was done by PYMOL. Superposition of the modeled ATX Zinc finger domain structure on the known structures of FYVE-Zinc finger domain complexed with the inositol 1,3-bisphosphate (1HYI) resulted in a good fit of the backbones (ATX 609–644, 652–660; FYVE-Zinc finger 8–43, 54–67). To locate the ligand binding site of PHD_{ATX}, structural comparisons were done between PHD_{ATX}, the solution structure of the $FYVE_{EEA1}$ domain complexed with PI3P (8).

1. Stevenson, J., M., Perera, I., Y., Heilmann, I., Persson, S. & Boss, W. F. (2000) *Trends Plant Sci.* **5,** 252–258.

2. Jasencakova, Z., Meister, A., Walter, J., Turner, B. M. & Schubert, I. (2000) *Plant Cell* **12,** 2087–2100.

3. Misra, S. & Hurley, J. H. (1999) *Nucleic Acids. Res.* **31,** 3381–3385.

4. Zhang, G., Kazanietz, M. G., Blumberg, P. M. & Hurley, J. H. (1995) *Cell* **81,** 917–924.

5. Schwede, T., Kopp, J., Guex, N. & Peitsch, M. C. (2003) *Cell* **97,** 657–666.

6. Bates, P. A., Kelley, L. A., MacCallum, R. M. & Sternberg, M. J. E. (2001) *Proteins* **5,** 39–46.

7. Collaborative Computational Project No. 4 (1994) *Acta Crystallogr. D* **50,** 760–763.

8. Kutateladze, T. & Overduin, M. (2001) *Science* **291,** 1793–1796.

9. Dowler, S., Kular, G. & Alessi, D. (2002) *Sci. STKE* **129,** PL6.